Article

Current Biology

Distinct oscillatory neural rhythms support representational precision and confidence in working memory

Highlights

- Humans track trial-by-trial fluctuations of working memory uncertainty
- Alpha-band activity carries probabilistic representations of memorized locations
- The precision of memory representations in alpha activity predicts uncertainty
- Beta-band activity encodes a scalar confidence signal that persists across trials

Authors

Yang Di, Xingwei An, Hsin-Hung Li

Correspondence

li.14492@osu.edu

In brief

Di et al. show that two distinct oscillatory neural rhythms encode different aspects of working memory uncertainty. Alpha-band activity carries probabilistic memory representations whose precision predicts behaviorally reported uncertainty, whereas beta-band activity carries a scalar confidence signal that persists across task epochs and trials.

Di et al., 2026, Current Biology *36*, 1–10
October 5, 2026
https://doi.org/10.1016/j.cub.2026.08.041

CellPress

Please cite this article in press as: Di et al., Distinct oscillatory neural rhythms support representational precision and confidence in working memory, Current Biology (2026), https://doi.org/10.1016/j.cub.2026.08.041

Current Biology

CellPress

Article

Distinct oscillatory neural rhythms support representational precision and confidence in working memory

Yang Di,[1,2] Xingwei An,[1] and Hsin-Hung Li[2,3,*]
[1]Academy of Medical Engineering and Translational Medicine, Tianjin University, Tianjin 300072, China
[2]Department of Psychology, The Ohio State University, Columbus, OH 43201, USA
[3]Lead contact
*Correspondence: li.14492@osu.edu
https://doi.org/10.1016/j.cub.2026.08.041

SUMMARY

Working memory enables the maintenance of information to guide behavior, yet its representations are inherently noisy and variable. To act effectively, observers must track the uncertainty of their own memory. However, the neural mechanisms supporting uncertainty representations in working memory remain poorly understood, particularly at the level of neural dynamics. Here, we combined electroencephalography (EEG) with a spatial visual working memory task that elicited trial-by-trial uncertainty reports to investigate how oscillatory activity encodes memory uncertainty. We identified two forms of uncertainty supported by distinct oscillatory neural activity. Using a probabilistic encoding-decoding model, we found that memory content can be reconstructed from alpha-band activity and that the precision of these representations predicts subsequent uncertainty reports, consistent with probabilistic mnemonic representations. In parallel, beta-band activity contained a scalar, magnitude-based representation of uncertainty. This signal exhibited slow, persistent dynamics across task epochs and tracked uncertainty reports for both the current and previous trials. Together, these findings show that the human brain multiplexes two forms of memory uncertainty, representational precision and a scalar confidence signal, across distinct oscillatory rhythms, providing a neural dynamical account of metacognitive access to working memory.

INTRODUCTION

Working memory enables neural representations to be maintained beyond the moment of perception and to guide behavior. A hallmark of working memory is that its quality fluctuates over time.[1–3] Even when identical stimuli are encoded repeatedly, the neural activity supporting mnemonic representations remains variable and noisy, rendering working memory uncertain. Adaptive behavior therefore requires access not only to remembered content but also to its uncertainty, enabling individuals to evaluate how much their memory can be trusted. This metacognitive process is sometimes referred to as metamemory or meta-WM.[4–7]

While the neural basis of uncertainty and metacognitive judgments has been extensively studied in perception[8–10] (reviewed in previous studies[11–17]), only recently have studies begun to investigate how the human brain represents uncertainty in working memory. Recent human fMRI studies have shown that the quality of mnemonic representations in the visual and intraparietal cortex correlates with behavioral uncertainty reports.[18,19] However, metacognition likely relies on multiple signals rather than solely on instantaneous memory fidelity. For example, uncertainty reports may be influenced by performance in recent trial history.[20,21] It remains unclear whether distinct formats of uncertainty are encoded by common neural representations or by multiple specialized codes. Moreover, the neural dynamics underlying the formation of memory uncertainty remain largely unexplored. In particular, it is unknown whether uncertainty is represented in oscillatory neural activity, a ubiquitous and temporally structured feature of population dynamics, despite its established role in working memory and higher-order cognition.

Oscillatory neural activity reflects coordinated population dynamics across frequency bands, each linked to distinct computations or cognitive functions,[22,23] making it well suited to support different aspects of metacognitive functions. Here, we test whether and how two forms of uncertainty representation in working memory, representational precision and a scalar confidence signal, are carried by distinct oscillatory dynamics.

First, working memory uncertainty may arise from the precision of the mnemonic representations themselves. In this view, neural populations maintaining memory content encode not only a point estimate but also probabilistic information whose precision reflects memory quality. In human scalp electroencephalogram (EEG) recordings, alpha-band oscillations (~8–13 Hz) have been repeatedly implicated in visual working memory. During the memory delay, alpha activity is prominent and has been associated with spatial attention, suppression of irrelevant information, and maintenance of spatial representations.[24–27] Critically, the content of working memory can be reconstructed from alpha-band topography,[28–33] indicating that alpha-band activity carries mnemonic content. However, prior

Please cite this article in press as: Di et al., Distinct oscillatory neural rhythms support representational precision and confidence in working memory, Current Biology (2026), https://doi.org/10.1016/j.cub.2026.08.041

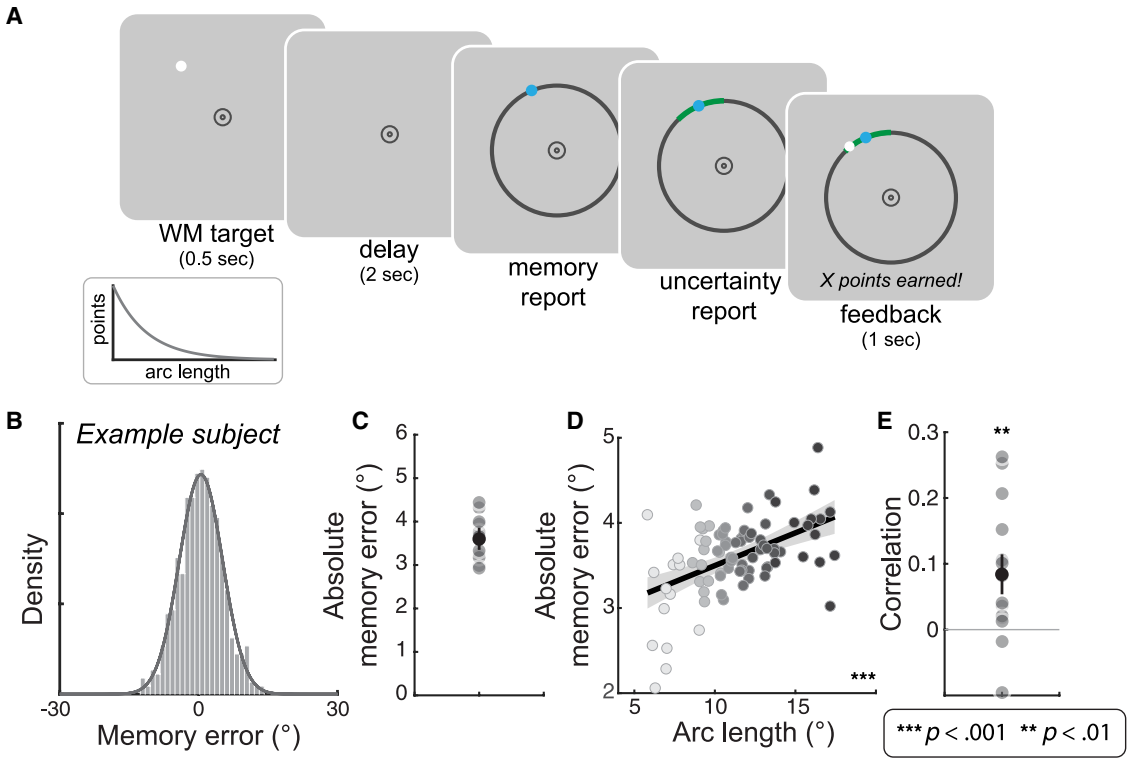

Figure 1. Procedures and behaviors

(A) Procedures. Each trial started with the target at a random polar angle followed by a delay period, during which participants maintained fixation and were required to remember the target location. After the delay, participants first reported their memory by clicking on the screen and reported their uncertainty by adjusting the length of an arc. Feedback was subsequently provided as a dot at the true target position. If the target position fell within the arc, points were awarded accordingly based on the reward policy (lower left inset).

(B) The distribution of behavioral memory error from an example participant. The gray line represents the best-fit von Mises distribution.

(C) Absolute behavioral memory error. The light gray dots represent individual participants. The black dot with the error bar represents the group mean ± SEM.

(D) Absolute memory error plotted against the arc length (reported uncertainty). Different gray levels indicate different bins sorted by arc length within each participant (8 bins per participant). The black line represents the best linear fit.

(E) The correlation between absolute memory error and arc length for individual participants (gray dots). The black dot represents the group average. The error bar represents ±SEM.

studies rarely examined how decoded memory content relates to subjective uncertainty or trial-by-trial memory error. Consequently, whether alpha-band activity encodes uncertainty of working memory remains unknown.

Second, metacognitive evaluation of working memory may rely on a different form of uncertainty representation. In addition to representational precision, neural populations may encode uncertainty as a simpler scalar signal that summarizes overall confidence level. Such signals could guide uncertainty reports or subsequent behavior without representing the remembered stimulus features themselves. Moreover, this signal may represent a confidence level that persists across trials or task epochs without interfering with ongoing sensory inputs or trial-wise mnemonic representations. Note that although confidence and uncertainty can have distinct theoretical interpretations,[34] in the context of the scalar signal, we do not distinguish between the two terms for the present continuous estimation task.

In this study, we recorded EEG signals while human participants performed a spatial working memory task that required explicit trial-by-trial uncertainty reports. We found that uncertainty derived from the memory representations in alpha-band activity predicted subsequent subjective uncertainty judgments. In parallel, we identified a scalar signal expressed in beta-band activity that tracked uncertainty across task epochs and across trials. Together, these findings show that working memory uncertainty is supported by multiple neural codes across oscillatory dynamics, with representational precision and a scalar confidence signal carried by distinct frequency bands.

RESULTS

To explicitly probe working memory uncertainty that guides decisions, we adapted a paradigm that incentivized participants to report their memory uncertainty in a betting game.[18,35,36] In a spatial visual working memory task, a brief target dot (0.5 s, fixed at 10° eccentricity) was presented at a pseudo-random polar angle on each trial (Figure 1A). The target was followed by a 2-s delay period while participants maintained fixation at the central fixation. After the delay, participants first reported the remembered location using a mouse click. Following this

Please cite this article in press as: Di et al., Distinct oscillatory neural rhythms support representational precision and confidence in working memory, Current Biology (2026), https://doi.org/10.1016/j.cub.2026.08.041

response, an arc representing a confidence interval was displayed on the screen, centered at the reported location. Participants adjusted the arc length to report their uncertainty about the remembered position. At the end of each trial, a feedback dot appeared at the true target location. Participants earned points if the target fell within the arc and earned zero points otherwise. When earned, the number of points decreased as a function of arc length. This task structure incentivized participants to report their memory uncertainty through the arc length.[35,36]

Participants' memory reports were centered on the target location when expressed as memory error (Figure 1B). As expected, given the presence of a single target and the short delay duration, memory reports were quite precise (Figure 1C). Importantly, reported arc length, an explicit measure of subjective uncertainty, increased with the magnitude of memory error (Figures 1D and 1E), demonstrating that participants have metacognitive access to trial-by-trial fluctuations in working memory precision.[18,35,36]

Mnemonic representations in alpha-band activity reflect memory uncertainty

One potential source of memory uncertainty lies in the precision of the underlying mnemonic representations. Rather than a single point estimate, memory representations may take a probabilistic format that inherently conveys uncertainty. We obtained a theoretically grounded neural measure of uncertainty by decoding working memory content from alpha-band activity with a generative model-based Bayesian decoder.[9,18,37] In a cross-validation procedure, training data were used to construct a generative model that maps stimulus location (polar angle) to EEG activity patterns. The model assumed that multi-electrode EEG activity follows a multivariate normal distribution, with a mean that depends on the spatial tuning function of each electrode and a covariance that characterizes neural and measurement noise (STAR Methods). Once the model was established, we inferred the target location on each single trial in the test set by computing a posterior distribution over locations given the observed EEG activity pattern $p(s|\mathbf{b})$ through Bayesian inference (where s represents location and $\mathbf{b}$ represents alpha activity pattern; Figure 2A). Interpreting these distributions as the mnemonic representations available to the observers, we used the posterior mean as a readout of remembered location and its width (standard deviation) as a neural index of memory uncertainty, which could guide the uncertainty report (Figure 2A).

We conducted a planned analysis using a predefined 1-s time window centered at the middle of the memory delay (0.5 to 1.5 s from delay onset) and computed the power spectral density within this window with Welch's method (STAR Methods). Applying the Bayesian decoder to the alpha power (8–13 Hz), we found that the spatial location (polar angle) held in working memory was decodable, as indicated by the absolute decoding errors (mean = 80.5°, $t(13) = 6.42$, $p < 0.001$; Figures 2B and 2C). For the majority of participants (12 out of 14), decoding errors exhibited clustering around 0°, indicating above-chance decoding (Figure 2B for an example subject; see individual results in Figure S1). Moreover, the (signed) decoding error significantly correlated with the (signed) memory error (Figures 2D and 2E), suggesting a close correspondence between the memory representations in the alpha band and behavioral reports.

We next investigated whether neural uncertainty of working memory predicts explicit behavioral uncertainty reports. Behavioral uncertainty reports (arc length) increased with the uncertainty derived from the decoded memory content from the alpha band ($t(13) = 2.32$, $p = 0.04$; Figures 2F and 2G). This relationship indicates that the memory representations held in alpha-band activity not only support memory reports but also that their uncertainty can inform trial-wise uncertainty reports. This correlation between decoded and reported uncertainty remained significant in a permutation test in which the reported uncertainty was permuted by shuffling run identities while preserving the trial order within each run (permutation test, $p = 0.002$; Figure S2A; STAR Methods). This analysis indicates that the observed correlation cannot be explained by run-specific temporal structure in the uncertainty reports.[38] In addition, we found that the decoded uncertainty correlated with decoding performance, indexed by the absolute decoding error, a signature for a well-behaved probabilistic decoder ($t(13) = 3.16$, $p = 0.008$; Figures 2H and 2I).

We applied the same analyses to theta (2–7 Hz) and beta power (14–30 Hz) within the same time window. No reliable decoding was observed in the theta band. In the beta band, the target location was decodable, but the performance was worse than that in alpha (Figure S3A). In addition, beta-band decoding error did not correlate with behavioral memory error, nor did its decoded uncertainty correlate with reported uncertainty (Figures S3B and S3C). We also tested a decoder that used both the real and imaginary components of the signals, rather than the power, as features.[39] Although this doubled the number of input features, the decoder yielded chance-level performance across all frequency bands tested (Figure S3D). These results suggest that target locations are primarily represented in the power of the oscillatory activity and that the Bayesian decoder does not naturally recover the nonlinear transformation from the real and imaginary components to the power.

Beta-band activity encodes a scalar representation of uncertainty

While the precision of mnemonic representations provides a trial-specific and momentary source of uncertainty, it may not be the sole neural substrate supporting metacognitive judgments. Representational precision, as well as other cues, could be integrated and converted into a simpler format, representing uncertainty or confidence as a scalar or a magnitude variable. This notion follows the previous findings that regional activity levels or neural population response scales with confidence ratings or opt-out behaviors in perceptual decisions.[12,14–16,40] To assess the neural basis of a scalar representation of uncertainty, we applied ridge regression to predict trial-by-trial uncertainty reports (arc length) directly from multivariate band-limited power within the same time window (0.5 to 1.5 s from delay onset) during the memory delay. By correlating the predicted (cross-validated) arc length from the ridge regression and the actual reported arc length, we found that beta-band activity reliably predicted the uncertainty report ($t(13) = 2.92$, $p = 0.012$), whereas other frequency bands showed chance-level performance (Figures 3A and 3B). This correlation remained significant in a run-shuffling permutation test (permutation test, $p = 0.002$; Figure S2B), indicating that it cannot be explained by run-specific temporal structure in the uncertainty reports.

Please cite this article in press as: Di et al., Distinct oscillatory neural rhythms support representational precision and confidence in working memory, Current Biology (2026), https://doi.org/10.1016/j.cub.2026.08.041

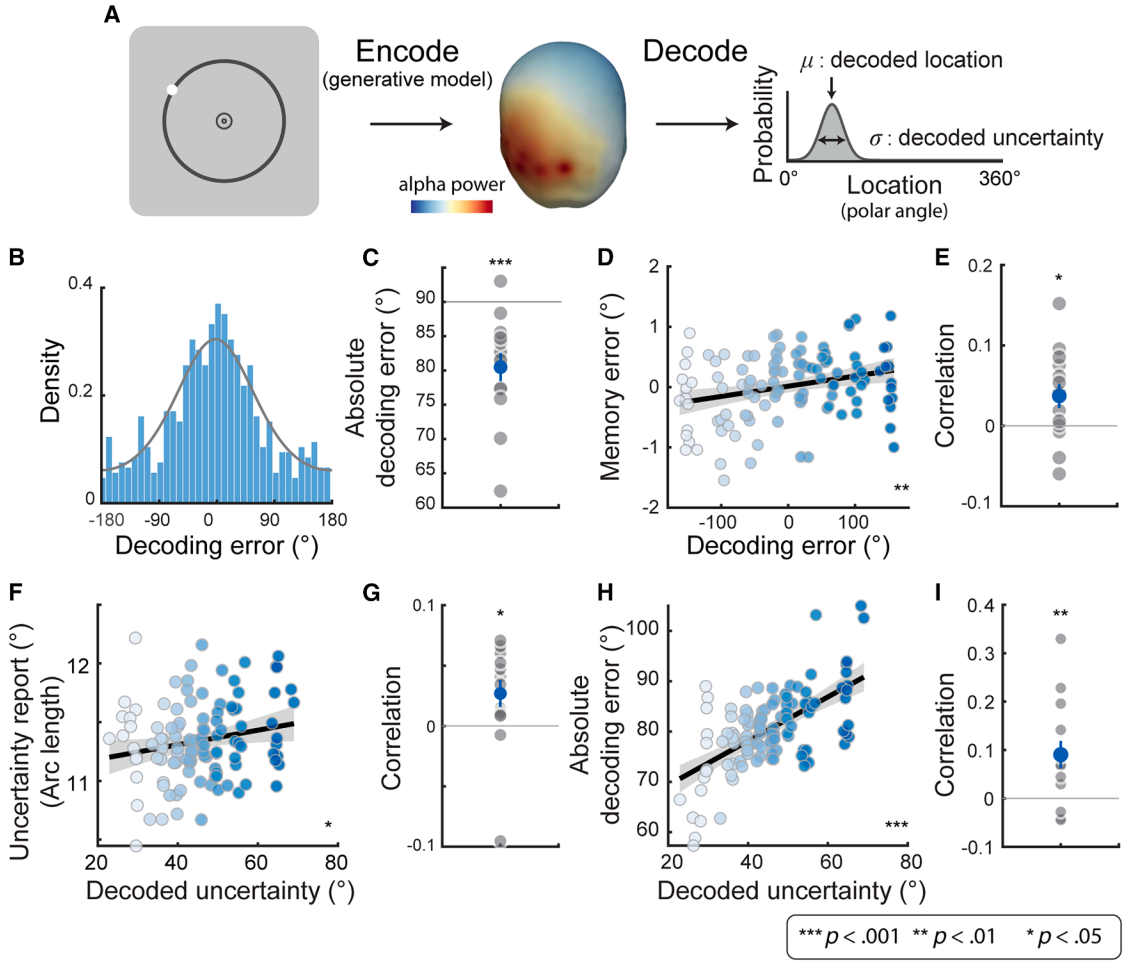

Figure 2. Probabilistic decoding of mnemonic representations from alpha-band activity

(A) Encoding model: we used the training data to build an encoding model, which modeled the multivariate alpha activity as a function of the polar angle of the target. Decoding: after fitting the encoding model, target location was inferred for each single trial in the test set using Bayesian inference. The posterior mean was taken as the decoded location, and the posterior standard deviation as the decoded uncertainty.

(B) Decoding error histogram from an example participant. The gray line represents the best-fit von Mises.

(C) Absolute decoding error for individual participants (gray dots). The horizontal gray line represents the chance level (90°). The blue dot represents the group average, and the error bar represents ±SEM.

(D) Memory error plotted against decoding error. Different colors represent different bins sorted by decoding error within each participant (8 bins/colors per participant). The black line represents the best linear fit, and the shaded area indicates 95% confidence interval (CI).

(E) Correlation between memory error and decoding error for individual participants (gray dots). The blue dot represents the group average. The error bar represents ±SEM.

(F) Uncertainty report plotted against decoded uncertainty. Different colors indicate different bins sorted by decoded uncertainty within each participant. The black line represents the best linear fit.

(G) Correlation between uncertainty report and decoded uncertainty for individual participants (gray dots). The blue dot represents the group average. The error bar represents ±SEM.

(H) Absolute decoding error plotted against decoded uncertainty. Different colors represent different bins sorted by decoded uncertainty within each participant. The black line represents the best linear fit.

(I) Correlation between absolute decoding error and decoded uncertainty for individual participants (gray dots). The blue dot represents the group average, and the error bar represents ±SEM.

See also Figures S1, S2A, and S3.

Distinct time courses and cortical origins of two forms of uncertainty

To compare the two forms of uncertainty signals we observed, the representational precision from the alpha band and the scalar signal in the beta band, we conducted time-resolved decoding and source reconstruction. Decoded uncertainty (derived from Bayesian decoding of target location from alpha power) quickly decreased after stimulus onset, indicating decodable information (Figure 4A). Target location remained decodable throughout the delay, as reflected by both decoded uncertainty (Figure 4A) and absolute decoding error (Figure S4A). The correlation between decoded uncertainty and behavioral uncertainty

Please cite this article in press as: Di et al., Distinct oscillatory neural rhythms support representational precision and confidence in working memory, Current Biology (2026), https://doi.org/10.1016/j.cub.2026.08.041

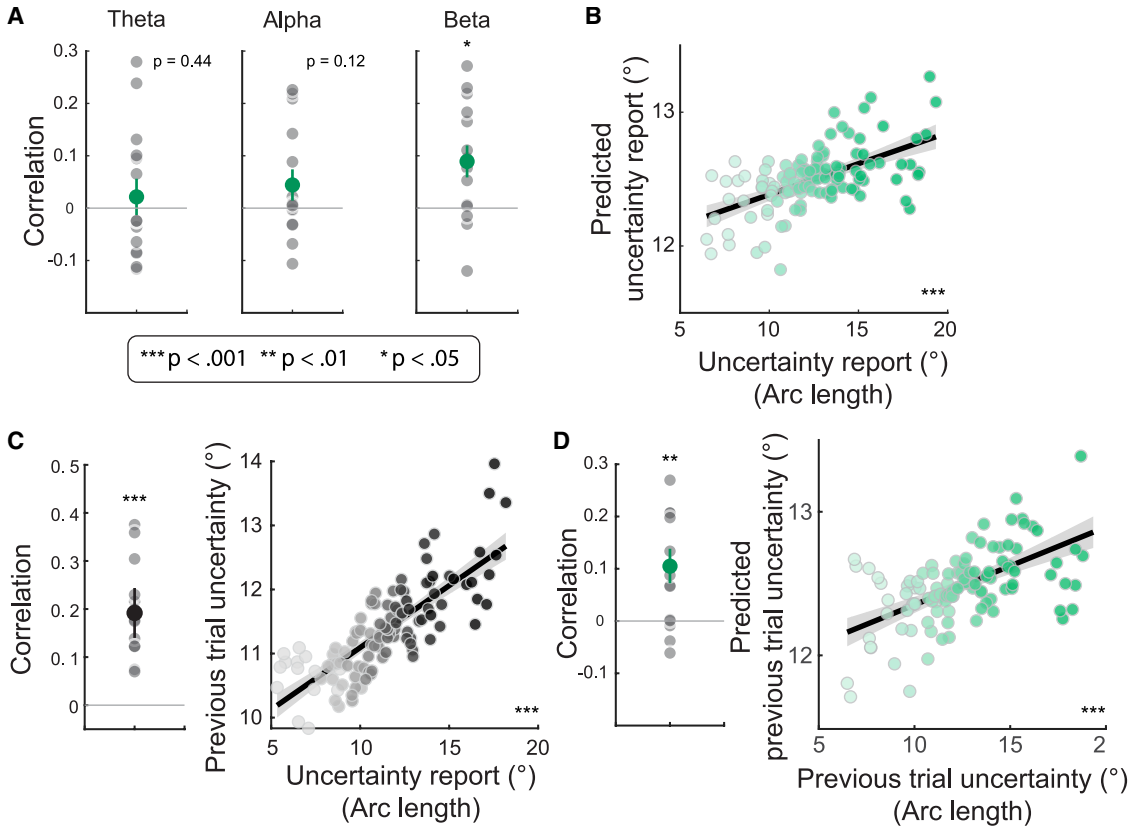

Figure 3. Scalar representation of uncertainty from beta-band activity

(A) Correlations between the uncertainty report and those predicted (cross-validated) by ridge regressions using the power of different frequency bands. The gray dots are correlation coefficients for individual participants. The green dot indicates the group mean; error bars denote ±SEM.

(B) Predicted uncertainty report (cross-validated) from ridge regressions using beta-band activity plotted against the uncertainty report. The black line shows the best linear fit, and the shaded area indicates 95% CI.

(C) Serial dependence of behavioral uncertainty reports. Correlation between uncertainty reports on the current trial and the previous trial. Data are plotted in the same format as (A) and (B).

(D) Correlation between uncertainty reports on the previous trial and those predicted by a ridge regression trained to predict previous-trial uncertainty reports using the beta-band activity from the current trial. Data are plotted in the same format as (A) and (B).

See also Figure S2B.

reports only emerged during the middle of the delay in a relatively short and late time window (Figure 4B). Interestingly, when the same Bayesian decoder was applied to the time-domain EEG voltage signals, the remembered location was decodable only during stimulus presentation and fell to chance during the memory delay (Figure S4B).

When ridge regression was used to directly predict reported arc length, beta-band activity showed above-chance prediction throughout the entire trial, even before stimulus onset (Figure 4D). This pattern indicates the presence of a persistent, slowly evolving confidence signal across trials and task epochs. Consistent with this interpretation, behavioral uncertainty reports exhibited serial dependence, with behaviorally reported uncertainty on the current trial correlated with that of the previous trial (Figure 3C). To test whether beta-band activity carries information about past uncertainty, we trained a ridge regression where we used the previous trial's reported arc length as the dependent variable. We found that beta-band activity in the current trial can reliably "predict" uncertainty from the previous trial (Figure 3D).

We performed source reconstruction on band-limited power during the 1-s time window in the middle of the memory delay (0.5 to 1.5 s after delay onset). EEG time series were first projected onto the cortical surface, and trial-wise band-limited power was then computed at each cortical vertex. As we have shown above that alpha-band activity contributes to memory uncertainty by representing the memorized target location, we examined cortical regions where trial-wise alpha power correlated with the target location (STAR Methods). This analysis revealed a cluster on the left parieto-occipital sulcus whose alpha power varied with the remembered location (Figure 4C). Notably, this region broadly overlaps with areas V3AB and IPS0 in the dorsal visual and posterior parietal cortex, where our previous fMRI studies using a similar task identified the strongest location decoding and the strongest relationship between decoded uncertainty and behavioral uncertainty reports.[18,19,41]

By contrast, for beta-band activity, we correlated beta power at each cortical vertex with the reported arc length. This analysis revealed clusters at the precentral and postcentral sulci and

Please cite this article in press as: Di et al., Distinct oscillatory neural rhythms support representational precision and confidence in working memory, Current Biology (2026), https://doi.org/10.1016/j.cub.2026.08.041

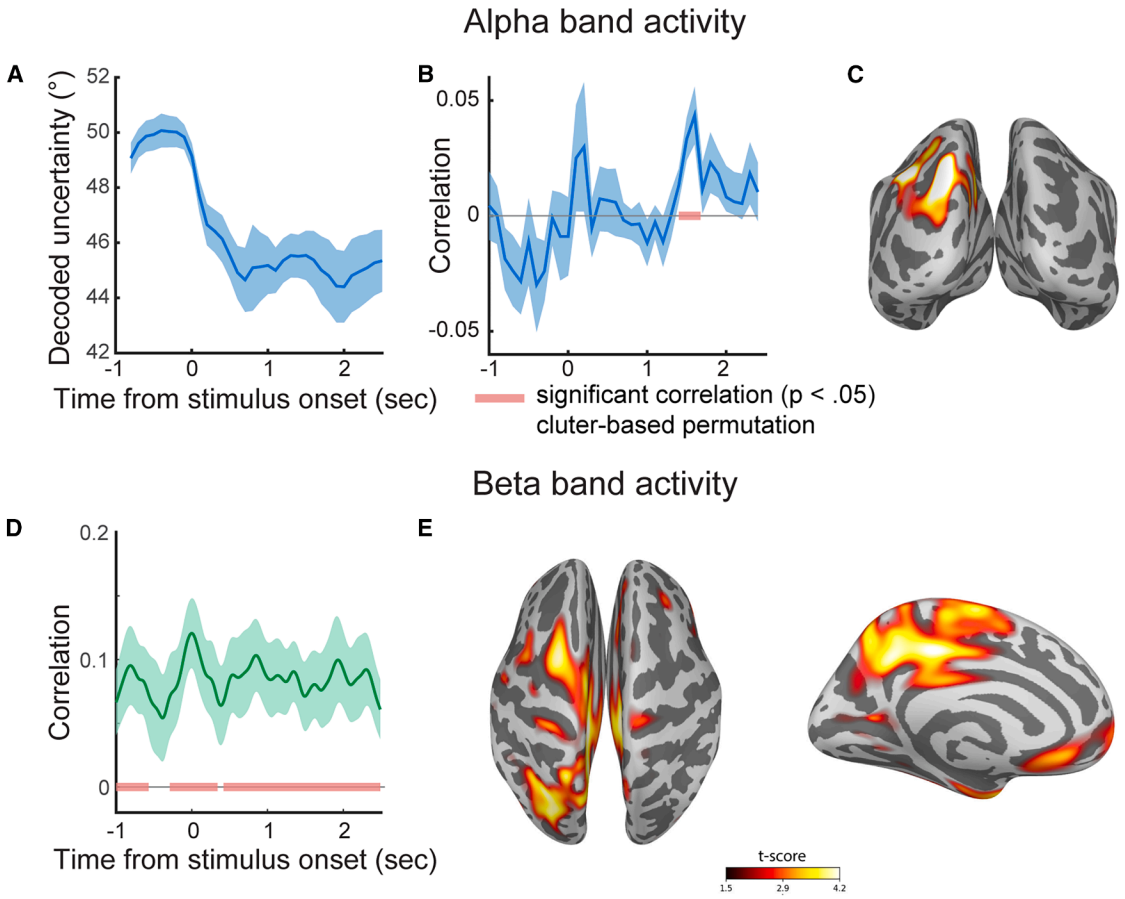

Figure 4. Time-resolved analysis and source reconstructions for two types of uncertainty signals

(A) Time-resolved decoded uncertainty from alpha activity. The blue line represents the group average, and the blue shaded interval shows ±SEM.

(B) Correlation between (cross-validated) decoded uncertainty from the alpha-band activity by the Bayesian decoder and reported uncertainty (arc length). The red line indicates a significant cluster.

(C) Source reconstruction for alpha-band activity (power) during the 0.5–1.5 s time window from the delay onset. The warm color represents cortical vertices where alpha-band activity correlates with target location (see source localization in the STAR Methods).

(D) Correlation between the (cross-validated) predicted uncertainty report by the beta-band activity and the actual uncertainty report. The red lines indicate significant clusters. The green line represents the group average, and the green shaded area indicates ±SEM.

(E) Source reconstruction for beta-band activity (power) during the 0.5–1.5 s time window from the delay onset. The warm color represents cortical vertices where beta-band activity correlates with reported uncertainty (arc length).

See also Figures S4 and S5.

additional medial clusters around the precuneus, paracentral lobule, and prefrontal cortex, where beta power correlated with reported uncertainty (Figure 4E). We performed the same analysis for alpha-band power but did not identify any cortical sources showing a correlation with reported arc length. These findings are consistent with the previous results that scalar uncertainty signals are primarily associated with beta-band activity.

The time course of the beta-band signals and their localization, which included sensorimotor cortex among other regions, raise the possibility that they reflect motor responses associated with arc-length adjustment. We performed several analyses to evaluate this interpretation. First, the initial arc length was uniformly randomized between 0° and 20°. This range covered well the observed distribution of reported arc lengths (Figure S5A), reducing the coupling between reported uncertainty and motor demands. Second, we examined the relationship between reported arc length and adjustment time (the time required to complete the uncertainty report after the location report had been finalized) and found no significant correlation (mean correlation = −0.018, $p = 0.63$). Third, scalar uncertainty could still be predicted from the beta-band activity during the location-report period ($t(13) = 3.75$, $p = 0.002$; Figure S5B), when participants used a mouse to click on the remembered location—a motor act distinct from the button presses used to adjust the arc length. Lastly, we used eye-related measures, including gaze positions, gaze velocity, and pupil size, to predict the reported arc length. The correlation between predicted and reported arc length was weak compared with the prediction by beta band and was not significant at any time point tested (Figure S5C). Together, these results argue against the interpretation that the beta-band activity is solely

Please cite this article in press as: Di et al., Distinct oscillatory neural rhythms support representational precision and confidence in working memory, Current Biology (2026), https://doi.org/10.1016/j.cub.2026.08.041

driven by the motor responses related to uncertainty reports and instead support the view that it reflects a decision-related internal state coupled with subjective uncertainty or confidence.

DISCUSSION

In this study, we identified two distinct but coexisting oscillatory rhythms that encode different aspects of memory uncertainty. Alpha-band activity represents the memorized location while concurrently carrying probabilistic information, enabling the precision of the mnemonic representation to guide uncertainty reports. In parallel, beta-band activity carries a scalar representation of uncertainty that tracks a slow-evolving confidence level across task epochs and trials.

Alpha-band activity has been widely linked to spatially specific representations in working memory and attention. In particular, the topography of alpha power can be used to decode the remembered location during delay periods[29–33] or the locus of spatial attention.[27] Extending this literature beyond decoding the target identity, we show that trial-by-trial decoding error predicts subsequent behavioral error. More importantly, the precision of the memory representations expressed in alpha-band activity is predictive of subjective uncertainty reports, linking alpha-band activity to metacognitive evaluation of memory quality.

Our recent fMRI studies showed that working memory representations reconstructed from blood-oxygen-level-dependent (BOLD) activity in the visual and parietal cortex predict both memory reports and uncertainty,[18,19] consistent with the idea that population codes jointly represent an encoded item and its uncertainty.[8,42,43] The present findings extend this framework by showing that probabilistic information is also expressed in alpha-band activity, indicating that uncertainty-related population codes can be accessed across measurement modalities and temporal scales. Alpha-band signals recorded with EEG reflect large-scale synaptic and transmembrane population dynamics, closely related to local field potentials, and have been widely interpreted as inhibitory modulation that shifts cortical excitability.[44–47] Consistent with this view, alpha power is inversely related to BOLD responses during stimulus encoding, suggesting that the two provide complementary information about brain activity.[48] Together with our previous work measuring BOLD responses,[18,19] the present findings indicate that this complementarity extends beyond perception to working memory maintenance, with both track the content and uncertainty of mnemonic representations concurrently.

Our experimental design and analysis were intended to isolate neural signals related to working memory. The 2-s delay period was chosen to be comparable to, or longer than, those used in previous EEG studies of visual working memory.[29–32] In the analysis of a fixed time window (Figure 2), the EEG time series were first epoched from 0.5 to 1.5 s from delay onset, and the power spectral density was computed within this interval, minimizing contributions from sensory-evoked activity. Nevertheless, the behavioral measures, including memory error and uncertainty reports, likely reflect neural processes accumulated from stimulus encoding through behavioral response. Interestingly, decoded uncertainty from alpha-band activity emerged relatively late in the delay period (Figure 4B), suggesting that the observed neural and behavioral uncertainty may be influenced more strongly by variability arising during memory maintenance than by variability during stimulus encoding, which is likely to be smaller.

During metacognitive introspection, people rely on multiple sources of information beyond the instantaneous precision of the encoded representation. In our study, we observed a serial dependence in uncertainty reports, whereby the reported uncertainty on one trial correlated with that of the previous trial. Similar history effects or a more global evaluation of self performance has been reported in confidence judgments during categorical perceptual decisions.[20,21] Consistently, our findings point to the existence of a scalar confidence signal carried by beta-band activity, which persisted across different trial epochs and trials. This property is well suited for supporting the many behavioral roles attributed to confidence or uncertainty. Confidence has been shown to influence cognitive processing at multiple stages of decision-making, as early as how sensory evidence is accumulated[49] and as late as the execution of motor responses and behavioral reports.[50] Post-decision or post-feedback confidence is also known to affect decisions in the subsequent trial.[51] The slow temporal dynamics of the uncertainty representations in beta-band activity we observed is well-suited to serve such a role, which can continuously influence various phases within and across trials. This scalar confidence signal observed here may not be specific to visual working memory. A recent study on probability learning also reported a confidence signal in the beta band, even during the pre-trial period, suggesting that beta-band dynamics may reflect a more general confidence state.[52] While there are differences in the nature of these signals, our results are broadly in line with recent findings from non-human primate neurophysiology, reporting that pre-trial baseline activity in the dorsolateral prefrontal cortex (DLPFC) neural population is indicative of subsequent metacognitive judgments of working memory.[5]

In both conventional confidence-rating tasks and the continuous uncertainty-report paradigm here, observers must convert their internal evidence into an explicit behavioral report through a set of confidence criteria or a mapping function. Consequently, the reported uncertainty reflects not only the underlying uncertainty estimate but also the mapping process. Therefore, an alternative, though not mutually exclusive, interpretation is that beta-band activity reflects fluctuations in this criterion or mapping function. Because such fluctuations are likely driven by changes in confidence, the two accounts would be expected to produce highly similar behavioral and neural signatures, making them difficult to distinguish empirically. From this perspective, the beta-band activity reflects a broader internal state involved in transforming subjective uncertainty into confidence-guided behavior, rather than exclusively the mnemonic uncertainty alone.

The localization of the beta-band activity to regions around the pre- and postcentral sulcus is in line with previous work showing that beta-band activity in the sensorimotor cortex can index a confidence level estimated from an ideal observer model in motor-adaptation tasks[53] and with evidence that TMS disruption of the premotor cortex reduces serial dependence in visual estimation tasks, implicating these areas' contribution in maintaining information from one trial to the next.[54]

Earlier work has proposed that beta oscillations reflect the maintenance of the status quo, where beta-band activity is

associated with stabilizing the current motor state and suppressing changes in action plans. Related notions have been extended to various cognitive domains, suggesting that beta-band activity may support the stabilization of ongoing cognitive states or serve various top-down control functions in visual attention and working memory tasks.[22,55–59] The other account on beta-band activity has emphasized that beta oscillations also represent content-specific information, such as the parametric features of the items held in working memory.[60–62] Our findings reflect that these different interpretations on beta-band activity may be complementary. In our task, beta-band activity can be viewed as maintaining an internal state of uncertainty or confidence that persists across time. Importantly, the notion of "state" here is not a distinct mode devoid of content. Rather, like many latent variables in computational models of decision-making, the state carries a specific numerical value, much like the content maintained in working memory (e.g., the color or orientation of an object). In the present case, the maintained value is the magnitude of uncertainty itself.

RESOURCE AVAILABILITY

Lead contact

Further information and requests for information and resources should be directed to and will be fulfilled by the lead contact, Hsin-Hung Li (li.14492@osu.edu).

Materials availability

The study did not produce any new materials.

Data and code availability

- De-identified and pre-processed data have been deposited at https://osf.io/t96rn. They are publicly available as of the date of publication.
- All original code has been deposited at https://osf.io/t96rn and is publicly available as of the date of publication.
- Any additional information required to reanalyze the data reported in this paper is available from the lead contact upon request.

ACKNOWLEDGMENTS

H.-H.L. was supported by startup funds from The Ohio State University, USA.

AUTHOR CONTRIBUTIONS

Conceptualization, Y.D. and H.-H.L.; methodology, Y.D. and H.-H.L.; investigation, Y.D.; formal analysis, Y.D.; project administration, X.A. and H.-H.L.; supervision, X.A. and H.-H.L.; visualization, Y.D. and H.-H.L.; writing – original draft, Y.D. and H.-H.L.; writing – review & editing, Y.D., X.A., and H.-H.L.

DECLARATION OF INTERESTS

The authors declare no competing interests.

STAR★METHODS

Detailed methods are provided in the online version of this paper and include the following:

SUPPLEMENTAL INFORMATION

Supplemental information can be found online at https://doi.org/10.1016/j.cub.2026.08.041.

Received: April 8, 2026
Revised: July 15, 2026
Accepted: August 14, 2026

REFERENCES

1. Fougnie, D., Suchow, J.W., and Alvarez, G.A. (2012). Variability in the quality of visual working memory. Nat. Commun. *3*, 1229. https://doi.org/10.1038/ncomms2237.
2. van den Berg, R., Shin, H., Chou, W.-C., George, R., and Ma, W.J. (2012). Variability in encoding precision accounts for visual short-term memory limitations. Proc. Natl. Acad. Sci. USA *109*, 8780–8785. https://doi.org/10.1073/pnas.1117465109.
3. Bays, P.M., Schneegans, S., Ma, W.J., and Brady, T.F. (2024). Representation and computation in visual working memory. Nat. Hum. Behav. *8*, 1016–1034. https://doi.org/10.1038/s41562-024-01871-2.
4. Miyamoto, K., Osada, T., Setsuie, R., Takeda, M., Tamura, K., Adachi, Y., and Miyashita, Y. (2017). Causal neural network of metamemory for retrospection in primates. Science *355*, 188–193. https://doi.org/10.1126/science.aal0162.
5. Ning, C., Fu, G., Zhang, Y.-Y., Meyniel, F., and Wang, L. (2026). Macaque prefrontal cortex integrates multiple components for metacognitive judgments of working memory. Neuron *114*, 938–951.e7. https://doi.org/10.1016/j.neuron.2025.11.014.
6. Baird, B., Smallwood, J., Gorgolewski, K.J., and Margulies, D.S. (2013). Medial and lateral networks in anterior prefrontal cortex support metacognitive ability for memory and perception. J. Neurosci. *33*, 16657–16665. https://doi.org/10.1523/JNEUROSCI.0786-13.2013.
7. Hu, X., Zheng, J., Su, N., Fan, T., Yang, C., Yin, Y., Fleming, S.M., and Luo, L. (2021). A Bayesian inference model for metamemory. Psychol. Rev. *128*, 824–855. https://doi.org/10.1037/rev0000270.
8. Walker, E.Y., Cotton, R.J., Ma, W.J., and Tolias, A.S. (2020). A neural basis of probabilistic computation in visual cortex. Nat. Neurosci. *23*, 122–129. https://doi.org/10.1038/s41593-019-0554-5.
9. van Bergen, R.S., Ma, W.J., Pratte, M.S., and Jehee, J.F.M. (2015). Sensory uncertainty decoded from visual cortex predicts behavior. Nat. Neurosci. *18*, 1728–1730. https://doi.org/10.1038/nn.4150.
10. van Bergen, R.S., and Jehee, J.F.M. (2019). Probabilistic representation in human visual cortex reflects uncertainty in serial decisions. J. Neurosci. *39*, 8164–8176. https://doi.org/10.1523/JNEUROSCI.3212-18.2019.
11. Walker, E.Y., Pohl, S., Denison, R.N., Barack, D.L., Lee, J., Block, N., Ma, W.J., and Meyniel, F. (2023). Studying the neural representations of uncertainty. Nat. Neurosci. *26*, 1857–1867. https://doi.org/10.1038/s41593-023-01444-y.
12. Bang, D., and Fleming, S.M. (2018). Distinct encoding of decision confidence in human medial prefrontal cortex. Proc. Natl. Acad. Sci. USA *115*, 6082–6087. https://doi.org/10.1073/pnas.1800795115.
13. Kepecs, A., Uchida, N., Zariwala, H.A., and Mainen, Z.F. (2008). Neural correlates, computation and behavioural impact of decision confidence. Nature *455*, 227–231. https://doi.org/10.1038/nature07200.
14. Fleming, S.M., Huijgen, J., and Dolan, R.J. (2012). Prefrontal contributions to metacognition in perceptual decision making. J. Neurosci. *32*, 6117–6125. https://doi.org/10.1523/JNEUROSCI.6489-11.2012.

15. Kiani, R., and Shadlen, M.N. (2009). Representation of confidence associated with a decision by neurons in the parietal cortex. Science *324*, 759–764. https://doi.org/10.1126/science.1169405.

16. Vivar-Lazo, M., and Fetsch, C.R. (2026). Neural basis of concurrent deliberation toward a choice and confidence judgment. Nat. Neurosci. *29*, 159–170. https://doi.org/10.1038/s41593-025-02116-9.

17. Okazawa, G., Hatch, C.E., Mancoo, A., Machens, C.K., and Kiani, R. (2021). Representational geometry of perceptual decisions in the monkey parietal cortex. Cell *184*, 3748–3761.e18. https://doi.org/10.1016/j.cell.2021.05.022.

18. Li, H.-H., Sprague, T.C., Yoo, A.H., Ma, W.J., and Curtis, C.E. (2021). Joint representation of working memory and uncertainty in human cortex. Neuron *109*, 3699–3712.e6. https://doi.org/10.1016/j.neuron.2021.08.022.

19. Li, H.-H., Sprague, T.C., Yoo, A.H., Ma, W.J., and Curtis, C.E. (2025). Neural mechanisms of resource allocation in working memory. Sci. Adv. *11*, eadr8015. https://doi.org/10.1126/sciadv.adr8015.

20. Rouault, M., Dayan, P., and Fleming, S.M. (2019). Forming global estimates of self-performance from local confidence. Nat. Commun. *10*, 1141. https://doi.org/10.1038/s41467-019-09075-3.

21. Rahnev, D., Koizumi, A., McCurdy, L.Y., D'esposito, M., and Lau, H. (2015). Confidence leak in perceptual decision making. Psychol. Sci. *26*, 1664–1680. https://doi.org/10.1177/0956797615595037.

22. Fries, P. (2015). Rhythms for cognition: Communication through coherence. Neuron *88*, 220–235. https://doi.org/10.1016/j.neuron.2015.09.034.

23. Buzsáki, G., and Vöröslakos, M. (2023). Brain rhythms have come of age. Neuron *111*, 922–926. https://doi.org/10.1016/j.neuron.2023.03.018.

24. Spitzer, B., and Blankenburg, F. (2012). Supramodal parametric working memory processing in humans. J. Neurosci. *32*, 3287–3295. https://doi.org/10.1523/JNEUROSCI.5280-11.2012.

25. van Ede, F. (2018). Mnemonic and attentional roles for states of attenuated alpha oscillations in perceptual working memory: a review. Eur. J. Neurosci. *48*, 2509–2515. https://doi.org/10.1111/ejn.13759.

26. Jokisch, D., and Jensen, O. (2007). Modulation of gamma and alpha activity during a working memory task engaging the dorsal or ventral stream. J. Neurosci. *27*, 3244–3251. https://doi.org/10.1523/JNEUROSCI.5399-06.2007.

27. Samaha, J., Sprague, T.C., and Postle, B.R. (2016). Decoding and reconstructing the focus of spatial attention from the topography of alpha-band oscillations. J. Cogn. Neurosci. *28*, 1090–1097. https://doi.org/10.1162/jocn_a_00955.

28. Sutterer, D.W., Foster, J.J., Adam, K.C.S., Vogel, E.K., and Awh, E. (2019). Item-specific delay activity demonstrates concurrent storage of multiple active neural representations in working memory. PLoS Biol. *17*, e3000239. https://doi.org/10.1371/journal.pbio.3000239.

29. Foster, J.J., Bsales, E.M., Jaffe, R.J., and Awh, E. (2017). Alpha-band activity reveals spontaneous representations of spatial position in visual working memory. Curr. Biol. *27*, 3216–3223.e6. https://doi.org/10.1016/j.cub.2017.09.031.

30. Foster, J.J., Sutterer, D.W., Serences, J.T., Vogel, E.K., and Awh, E. (2016). The topography of alpha-band activity tracks the content of spatial working memory. J. Neurophysiol. *115*, 168–177. https://doi.org/10.1152/jn.00860.2015.

31. Bae, G.-Y., and Luck, S.J. (2018). Dissociable decoding of spatial attention and working memory from EEG oscillations and sustained potentials. J. Neurosci. *38*, 409–422. https://doi.org/10.1523/JNEUROSCI.2860-17.2017.

32. Bae, G.-Y. (2021). Neural evidence for categorical biases in location and orientation representations in a working memory task. Neuroimage *240*, 118366. https://doi.org/10.1016/j.neuroimage.2021.118366.

33. Bender, A., Zhao, C., Vogel, E., Awh, E., and Voytek, B. (2025). Differential representations of spatial location by aperiodic and alpha oscillatory activity in working memory. Proc. Natl. Acad. Sci. USA *122*, e2506418122. https://doi.org/10.1073/pnas.2506418122.

34. Pouget, A., Drugowitsch, J., and Kepecs, A. (2016). Confidence and certainty: distinct probabilistic quantities for different goals. Nat. Neurosci. *19*, 366–374. https://doi.org/10.1038/nn.4240.

35. Honig, M., Ma, W.J., and Fougnie, D. (2020). Humans incorporate trial-to-trial working memory uncertainty into rewarded decisions. Proc. Natl. Acad. Sci. USA *117*, 8391–8397. https://doi.org/10.1073/pnas.1918143117.

36. Yoo, A.H., Klyszejko, Z., Curtis, C.E., and Ma, W.J. (2018). Strategic allocation of working memory resource. Sci. Rep. *8*, 16162. https://doi.org/10.1038/s41598-018-34282-1.

37. van Bergen, R.S., and Jehee, J.F.M. (2021). TAFKAP: An improved method for probabilistic decoding of cortical activity. Preprint at bioRxiv. https://doi.org/10.1101/2021.03.04.433946.

38. Harris, K.D. (2020). Nonsense correlations in neuroscience. Preprint at bioRxiv. https://doi.org/10.1101/2020.11.29.402719.

39. Weiss, A., Chambon, V., Lee, J.K., Drugowitsch, J., and Wyart, V. (2021). Interacting with volatile environments stabilizes hidden-state inference and its brain signatures. Nat. Commun. *12*, 2228. https://doi.org/10.1038/s41467-021-22396-6.

40. Zylberberg, A., and Shadlen, M.N. (2025). A population representation of the confidence in a decision in the parietal cortex. Cell Rep. *44*, 115526. https://doi.org/10.1016/j.celrep.2025.115526.

41. Li, H.-H., Ma, W.J., and Curtis, C.E. (2026). Dynamics of working memory drift and information flow across the cortical hierarchy. Proc. Natl. Acad. Sci. USA *123*, e2518110123. https://doi.org/10.1073/pnas.2518110123.

42. Ma, W.J., Beck, J.M., Latham, P.E., and Pouget, A. (2006). Bayesian inference with probabilistic population codes. Nat. Neurosci. *9*, 1432–1438. https://doi.org/10.1038/nn1790.

43. Jazayeri, M., and Movshon, J.A. (2006). Optimal representation of sensory information by neural populations. Nat. Neurosci. *9*, 690–696. https://doi.org/10.1038/nn1691.

44. Jensen, O., and Mazaheri, A. (2010). Shaping functional architecture by oscillatory alpha activity: gating by inhibition. Front. Hum. Neurosci. *4*, 186. https://doi.org/10.3389/fnhum.2010.00186.

45. Mazaheri, A., and Jensen, O. (2010). Rhythmic pulsing: linking ongoing brain activity with evoked responses. Front. Hum. Neurosci. *4*, 177. https://doi.org/10.3389/fnhum.2010.00177.

46. Iemi, L., Chaumon, M., Crouzet, S.M., and Busch, N.A. (2017). Spontaneous neural oscillations bias perception by modulating baseline excitability. J. Neurosci. *37*, 807–819. https://doi.org/10.1523/JNEUROSCI.1432-16.2016.

47. Lange, J., Oostenveld, R., and Fries, P. (2013). Reduced occipital alpha power indexes enhanced excitability rather than improved visual perception. J. Neurosci. *33*, 3212–3220. https://doi.org/10.1523/JNEUROSCI.3755-12.2013.

48. Hermes, D., Nguyen, M., and Winawer, J. (2017). Neuronal synchrony and the relation between the blood-oxygen-level dependent response and the local field potential. PLoS Biol. *15*, e2001461. https://doi.org/10.1371/journal.pbio.2001461.

49. Rollwage, M., Loosen, A., Hauser, T.U., Moran, R., Dolan, R.J., and Fleming, S.M. (2020). Confidence drives a neural confirmation bias. Nat. Commun. *11*, 2634. https://doi.org/10.1038/s41467-020-16278-6.

50. Seideman, J.A., Stanford, T.R., and Salinas, E. (2018). Saccade metrics reflect decision-making dynamics during urgent choices. Nat. Commun. *9*, 2907. https://doi.org/10.1038/s41467-018-05319-w.

51. Urai, A.E., Braun, A., and Donner, T.H. (2017). Pupil-linked arousal is driven by decision uncertainty and alters serial choice bias. Nat. Commun. *8*, 14637. https://doi.org/10.1038/ncomms14637.

52. Meyniel, F. (2020). Brain dynamics for confidence-weighted learning. PLoS Comput. Biol. *16*, e1007935. https://doi.org/10.1371/journal.pcbi.1007935.

53. Tan, H., Wade, C., and Brown, P. (2016). Post-movement beta activity in sensorimotor cortex indexes confidence in the estimations from internal models. J. Neurosci. *36*, 1516–1528. https://doi.org/10.1523/JNEUROSCI.3204-15.2016.

54. de Azevedo Neto, R.M., and Bartels, A. (2021). Disrupting short-term memory maintenance in premotor cortex affects serial dependence in visuomotor integration. J. Neurosci. *41*, 9392–9402. https://doi.org/10.1523/JNEUROSCI.0380-21.2021.

55. Kilavik, B.E., Zaepffel, M., Brovelli, A., MacKay, W.A., and Riehle, A. (2013). The ups and downs of β oscillations in sensorimotor cortex. Exp. Neurol. *245*, 15–26. https://doi.org/10.1016/j.expneurol.2012.09.014.

56. Engel, A.K., and Fries, P. (2010). Beta-band oscillations–signalling the status quo? Curr. Opin. Neurobiol. *20*, 156–165. https://doi.org/10.1016/j.conb.2010.02.015.

57. Lundqvist, M., Herman, P., Warden, M.R., Brincat, S.L., and Miller, E.K. (2018). Gamma and beta bursts during working memory readout suggest roles in its volitional control. Nat. Commun. *9*, 394. https://doi.org/10.1038/s41467-017-02791-8.

58. Liljefors, J., Almeida, R., Rane, G., Lundström, J.N., Herman, P., and Lundqvist, M. (2024). Distinct functions for beta and alpha bursts in gating of human working memory. Nat. Commun. *15*, 8950. https://doi.org/10.1038/s41467-024-53257-7.

59. Buschman, T.J., Denovellis, E.L., Diogo, C., Bullock, D., and Miller, E.K. (2012). Synchronous oscillatory neural ensembles for rules in the prefrontal cortex. Neuron *76*, 838–846. https://doi.org/10.1016/j.neuron.2012.09.029.

60. Spitzer, B., and Haegens, S. (2017). Beyond the status quo: a role for beta oscillations in endogenous content (re)activation. eNeuro *4*. ENEURO.0170-17.2017. https://doi.org/10.1523/ENEURO.0170-17.2017.

61. Wimmer, K., Ramon, M., Pasternak, T., and Compte, A. (2016). Transitions between multiband oscillatory patterns characterize memory-guided perceptual decisions in prefrontal circuits. J. Neurosci. *36*, 489–505. https://doi.org/10.1523/JNEUROSCI.3678-15.2016.

62. Spitzer, B., and Blankenburg, F. (2011). Stimulus-dependent EEG activity reflects internal updating of tactile working memory in humans. Proc. Natl. Acad. Sci. USA *108*, 8444–8449. https://doi.org/10.1073/pnas.1104189108.

63. Delorme, A., and Makeig, S. (2004). EEGLAB: an open source toolbox for analysis of single-trial EEG dynamics including independent component analysis. J. Neurosci. Methods *134*, 9–21. https://doi.org/10.1016/j.jneumeth.2003.10.009.

64. Gramfort, A., Luessi, M., Larson, E., Engemann, D.A., Strohmeier, D., Brodbeck, C., Goj, R., Jas, M., Brooks, T., Parkkonen, L., et al. (2013). MEG and EEG data analysis with MNE-Python. Front. Neurosci. *7*, 267. https://doi.org/10.3389/fnins.2013.00267.

65. Pascual-Marqui, R.D. (2002). Standardized low-resolution brain electromagnetic tomography (sLORETA): technical details. Methods Find. Exp. Clin. Pharmacol. *24*, 5–12.

66. Berens, P. (2009). CircStat: AMATLABToolbox for circular statistics. J. Stat. Softw. *31*. https://doi.org/10.18637/jss.v031.i10.

67. Maris, E., and Oostenveld, R. (2007). Nonparametric statistical testing of EEG- and MEG-data. J. Neurosci. Methods *164*, 177–190. https://doi.org/10.1016/j.jneumeth.2007.03.024.

Please cite this article in press as: Di et al., Distinct oscillatory neural rhythms support representational precision and confidence in working memory, Current Biology (2026), https://doi.org/10.1016/j.cub.2026.08.041

CellPress

STAR★METHODS

KEY RESOURCES TABLE

REAGENT or RESOURCE	SOURCE	IDENTIFIER
Deposited data		
EEG data	This paper	https://osf.io/t96rn
Behavioral data	This paper	https://osf.io/t96rn
Software and algorithms		
MATLAB	MathWorks	https://www.mathworks.com/products/matlab.html
TAFKAP	van Bergen and Jehee [9,37]	https://github.com/jeheelab/TAFKAP

EXPERIMENTAL MODEL AND STUDY PARTICIPANT DETAILS

In this study, we recruited 14 participants (7 males; 22–28 years old). All participants were right-handed and had normal or corrected-to-normal vision. They provided written informed consent prior to the experiment. The study was approved by the Ethics Committee of Tianjin University in accordance with institutional guidelines.

METHOD DETAILS

Procedures

The experimental procedure was implemented using Psychophysics Toolbox Version 3 running on MATLAB R2017a. Each participant completed 20 runs, with each run consisting of 32 trials. The trials were separated by a 2–3 s inter-trial interval, during which the fixation point was in dark gray. At the beginning of each trial, the fixation point increased in brightness to indicate trial onset. Participants were required to maintain their gaze at the fixation point for 1 s. The target, a bright dot, was then presented for 500 ms. The eccentricity of the target was fixed at 10° visual angle, and its polar angle was pseudo-randomly selected from 32 equally spaced positions spanning the full 360° range. After target offset, participants continued to fixate for a 2 s memory delay period while minimizing blinks and eye movements.

At the end of the delay, a black ring appeared on the screen as a response cue. Participants first moved a cursor to report the remembered target location and could fine-tune their response using the Up and Down arrow keys on the keyboard. After finalizing their memory report by pressing the space bar on the keyboard, an arc with a random initial length appears on the screen, centered at the reported target location with equal extension on both sides. The initial arc length was uniformly sampled between 0° and 20°. This design was adopted from our previous studies using similar spatial working memory tasks[18] and was intended to minimize the deterministic relationship between the reported arc length and the motor actions required to produce the report. Participants adjusted the length of the arc using the Up and Down arrow keys on the keyboard with both sides of the arc changing simultaneously. They pressed the space key again to confirm the reported arc length. Finally, a feedback dot was presented at the true target location. Reward points were determined by the reported arc length and whether the true target position fell within the arc.

The reward was designed to incentivize well-calibrated uncertainty reports.[18] The number of points ($100e^{-0.08d}$, where d is the length of the arc) participants could earn decreased monotonically with the length of the reported arc, such that shorter arcs yielded higher potential rewards. However, points were awarded only if the true target location fell within the reported arc; otherwise, participants earned zero points. This created a trade-off between maximizing potential reward and ensuring sufficient coverage to include the target. The optimal strategy was to adjust the arc length according to one's subjective uncertainty or confidence in the memory report.[35,36]

EEG setup

EEG data were recorded using a Neuroscan SynAmps2 system with 62 Ag/AgCl electrodes placed according to the international 10–20 system. The EEG signals were sampled at 1000Hz, and electrode impedances were maintained below 5 kΩ throughout the recording. During each experiment, eye movements and pupil diameter were recorded using a Tobii eye tracker (Tobii Pro Spectrum) at a sampling rate of 600 Hz.

EEG preprocessing

EEG data were preprocessed using the EEGLAB toolbox[63] in MATLAB. The data were re-referenced to the average reference, notch-filtered at 50 Hz and band-pass filtered between 0.1 and 45 Hz, and resampled to 500 Hz. Bad trials were identified by visual inspection and excluded if they exhibited baseline drifts, sharp transients, or movement-related deflections. Independent component

Please cite this article in press as: Di et al., Distinct oscillatory neural rhythms support representational precision and confidence in working memory, Current Biology (2026), https://doi.org/10.1016/j.cub.2026.08.041

analysis (ICA) was then applied to remove ocular, muscle, and other stereotypical artifacts. In total, 8,960 trials were collected from 14 participants (640 trials per participant). After bad-trial exclusion, 8,546 trials were retained (exclusion rate ~4%).

For the fixed time-window analysis (Figures 2 and 3) and source localization (Figures 4C and 4E), we focused on the 1-s time window during the memory delay period (0.5 to 1.5 s from delay onset). Feature extraction was performed using the MNE-Python package.[64] A random signal typically has finite average power, allowing it to be described in terms of its average power spectral density (PSD) $S_x(f)$, which is defined as:

$$S_x(f) = \lim_{T\to\infty}\frac{1}{T}|X_T(f)|^2$$

where $X(\tau, f)$ is the Fourier transform of a finite time window, and T is the length. Here, the fixed-window (0.5 to 1.5 s from delay onset) PSD for different frequency bands was estimated using Welch's method with a Hann window, and FFT length was set to 256.

The time-resolved analyses were based on epochs ranging from −1 s to 2.5 s relative to stimulus onset (Figures 4A, 4B, and 4D). Time-frequency representations of the EEG signals were computed using the short-time Fourier transform (STFT), which characterizes the spectral content of a signal over time by applying the Fourier transform within successive short temporal windows. Given a signal $x(t)$, the STFT is computed by multiplying the signal with a sliding window function $w(t)$ centered at time T, and then performing a Fourier transform within that window:

$$X(\tau, f) = \int_{-\infty}^{\infty} x(t)w(t-\tau)e^{-i2\pi ft}\,dt$$

where f is frequency, and $w(t-\tau)$is a Hann window centered at time T. A Hann window of 500 ms (equivalent FWHM = 250 ms) was used, and the time window was advanced in 100-ms steps.

EEG Decoding

Bayesian decoding

We conducted Bayesian decoding using the TAFKAP algorithm[9,37] to perform Bayesian decoding, extracting working memory representations and quantifying their uncertainty in probabilistic terms. This method allowed us to read out both the remembered location and the associated memory uncertainty jointly for each single trial.

In the generative model, the multivariate EEG signal associated with a target location (polar angle) was modeled as a multivariate normal distribution. The expected response (mean) of each electrode was defined by its tuning curve, representing an electrode's response (e.g., alpha power) as a function of target polar angle.

The tuning function of each electrode $f(s)$ was modeled as a linear combination of eight basis functions $g_k(s)$, which evenly spaced the polar angle space. These basis functions were raised cosine functions

$$g_k(s) = \max\left(0, \cos\left(\frac{\pi}{180}(s-\phi_k)\right)\right)^5$$

where ϕ_κ is the center of the k-th basis. The activity of i-th electrode to given the stimulus s is modeled as

$$b_i(s) = \sum_{k=1}^{8} W_{ik}(g_k(s)+\eta_k)+\epsilon_i$$

where W_{ik} weights the k-th basis function's contribution to the i-th electrode's tuning curve. The η and ϵ are the basis-specific noise and electrode-specific noise respectively. The probability of measuring EEG activity pattern $\mathbf{b}$ given the stimulus s is then $p(\mathbf{b}|s;\theta) = \mathcal{N}(f(s), \Omega)$. Where the model parameters θ are the basis function weights W and covariance matrix Ω. Here, the covariance is modeled as $\lambda\Omega_0 + (1-\lambda)\Omega_{\text{sample}}$.

To ensure a stable estimation of the covariance matrix, we modeled the covariance as a shrinkage of the sample covariance Ω_{sample} toward a target covariance matrix Ω_0. The free parameter λ determined the degree of shrinkage. Here, the target covariance matrix has a simple structure, computed as a weighted sum over a diagonal matrix, a rank-1 covariance matrix, and the covariance depending on the tuning weight matrix W of the voxels (see details in[9,37]).

Free parameters θ were estimated by maximizing the likelihood of the training data using leave-one-run-out cross-validation, in which the model was fit on all but one run and evaluated on the held-out run, iterating across all runs. We then decoded the target location on each trial in the test set based on the EEG activity pattern using Bayesian inference. Specifically, the posterior distribution was computed via Bayes' rule.

$$p(s|\mathbf{b};\theta) = \frac{p(\mathbf{b}|s;\theta)p(s)}{\int p(\mathbf{b}|s;\theta)p(s)\,ds}$$

We defined the mean and standard deviation of the trialwise posterior distribution as the decoded location and decoded uncertainty, respectively. We adopted the bagging procedure from the TAFKAP algorithm, in which the training data were bootstrapped to decode trials in the test set repeatedly, and the resulting posterior distributions were averaged until stable estimates were obtained.[37] For the time-resolved decoding in Figures 4A and 4B, the training and testing data are from the same time point.

Please cite this article in press as: Di et al., Distinct oscillatory neural rhythms support representational precision and confidence in working memory, Current Biology (2026), https://doi.org/10.1016/j.cub.2026.08.041

Ridge regression

To decode the neural activity that underlies scalar representations of uncertainty we used ridge regression to directly predict the report uncertainty (arc length) by the power of different frequency bands. Ridge regression is a regularized linear regression method by adding an L_2 penalty term to ordinary least squares (OLS), which shrinks the magnitude of the coefficients.

Given the arc length d and the EEG activity B, ridge regression estimates the coefficient vector w by minimizing $\| d - Bw\|^2 + \lambda \| w\|^2$ where λ is a non-negative regularization parameter controlling the degree of shrinkage applied to the regression coefficients. In our analysis, the regularization parameter was set to $\lambda = 10$.

Here, we used a leave-one-run-out cross-validation scheme, where run index according to the run order in the experiment. The data contain 20 runs, we trained the model on 19 runs to obtain the regression coefficients, and then used these coefficients to estimate the arc length on the remaining test run. For the time-resolved analysis in Figure 4D, the training and testing data are from the same time point.

For the analysis presented in Figure 3D, we treated the arc length reported in the previous trial d_{t-1} as the dependent variable, and used the beta-band activity in the current trial B_t to "predict" the previous arc length.

For the analysis presented in Figure S5B, the ridge regression model was applied to beta-band activity during the location-report period, defined as the interval from the end of the memory delay until the participant clicked the mouse to indicate the remembered target location. During this interval, participants used their dominant hand to move the mouse and report the target location, a motor action distinct from pressing the keyboard button with the fingers of the same hand to adjust the arc length. The mean duration of the location-report period was 2.44 s (SD across participants = 0.46 s).

Source Localization

We used Python-MNE to perform the source localization and visualization. sLORETA was used in Figures 4C and 4E to estimate cortical current density from EEG activity.[65] It belongs to the family of minimum-norm (MNE) inverse solutions.

The FreeSurfer fsaverage template was used to construct the source space (spacing = 'oct6'). The boundary element model (BEM), and the forward model were estimated for subsequent source reconstruction. The noise covariance matrix was estimated from the baseline interval (−0.5 to −0.05 s before the target onset). EEG signals were filtered at the frequency band of interest, cropped to the time window of interest (0.5 to 1.5 s from delay onset) and projected to source space. Cortical sources were estimated by inverting the forward model using sLORETA.

The resulting source estimates were originally in arbitrary units and reflect relative current density. In sLORETA, source estimates were further normalized by their expected variance, given by the diagonal of the resolution matrix. This normalization accounts for differences in sensitivity across cortical locations, with variance primarily determined by the forward model geometry (e.g., cortical depth and sensor configuration) and the noise covariance estimated from the baseline interval.

For each vertex, a Welch power spectral density was computed, and alpha/beta power was taken as the mean PSD over the corresponding frequency bands, and then log-transformed. For each subject and each vertex, a Pearson correlation was computed across trials between the power and the trial-wise behavioral variables. Specifically, we correlated alpha power with target location (polar angle) using the *circ_corrcl* function from the CircStat toolbox (Figure 4C),[66] and we correlated beta power with reported arc length (Figure 4E). The resulting correlation coefficients were Fisher z-transformed, and a one-sample t-test against zero was performed at each vertex (t-scores shown as the color map in Figures 4C and 4E).

Eye data analysis

Monocular pupil size and gaze position were recorded with a Tobii eye tracker (sampling 600 Hz) and epoched around memory-stimulus onset (−1000 to +2500 ms, resampled to a common 100-Hz grid). Pupil samples were excluded if pupil size fell outside 1–9 mm or if pupil size exceeded a threshold defined as 5 median absolute deviations above the median. Gaps up to 500 ms were linearly interpolated, and the trace was smoothed with a 50-ms moving average; gaze traces were cleaned by the same short-gap interpolation and converted from pixels to degrees of visual angle relative to fixation. A 200-ms window was stepped in 50 ms increments across the entire epoch, from -1 to 2.5 s relative to stimulus onset. At each window, the five features were computed as the within-window averages: mean pupil size (mm), mean horizontal and vertical gaze position relative to fixation (deg), mean radial gaze distance from fixation (deg), and mean gaze velocity (deg/s).

Within each participant we predicted the trial-wise confidence (arc length) report from the five eye-related features using ordinary least-squares regression evaluated with leave-one-run-out cross-validation, with features z-scored using training-fold statistics before fitting. Trials with any missing feature in the delay window or a missing uncertainty report were excluded. Cross-validated performance was quantified as the Pearson correlation between predicted and observed uncertainty report across held-out trials. At the group level, correlations were tested against zero with a one-sample t-test (Figure S5C).

QUANTIFICATION AND STATISTICAL ANALYSIS

In multiple figures, we illustrate the correlations between two variables (Figures 1E, 2E, 2G, 2I, and 3A). Pearson correlation coefficients were first computed within each participant. The resulting coefficients were Fisher z-transformed, and group-level significance was assessed using a one-sample t-test against zero. Alongside the single-trial correlations, we present scatter plots for visualization purposes. In these plots, each participant contributed eight data points (bins). For each participant, trials were first sorted according

Please cite this article in press as: Di et al., Distinct oscillatory neural rhythms support representational precision and confidence in working memory, Current Biology (2026), https://doi.org/10.1016/j.cub.2026.08.041

to the variable shown on the x-axis and then divided into eight bins with equal number of trials. For each bin, we computed the mean value of the variable on the y-axis across trials within that bin. Before pooling the data across participants, each participant's values were mean-centered to remove individual differences (for both x- and y-axis). As a result, between-subject variability did not contribute to the scatter plots.

For the correlation between decoded uncertainty and reported uncertainty reported in Figures 2F and 2G, we performed an alternative permutation test to rule out the possibility that the observed correlation was spuriously driven by temporal structure in the uncertainty reports that could be exploited by the decoder.[38] For each participant, the reported uncertainty was permuted by shuffling run identities while preserving the order of trials within each run (32 trials per run). We then computed the correlation between the permuted reported uncertainty and the decoded uncertainty from alpha-band activity. The resulting correlation coefficients were Fisher z-transformed and averaged across participants. This procedure was repeated 2,000 times to generate a null distribution of the group-averaged correlation coefficient. The empirical group-averaged correlation was then compared with this null distribution to compute a two-tailed p-value (Figure S5A). The same procedure was applied to test correlation between reported and predicted arc length by beta-band activity (Figure S5B).

Cluster-based permutation test was applied to test the time-resolved correlations reported in Figure 4. The procedures are based on those developed in Maris and Oostenveld.[67] For Figure 4B, we computed the correlation between decoded uncertainty (through Bayesian decoding of target location on alpha-band activity) and reported uncertainty within each participant. At each time point, group-level significance was evaluated using a one-sample t-test against zero. Adjacent time points with uncorrected significance ($p < 0.05$) were grouped into clusters, and cluster statistics were defined as the sum of t-values within each cluster. Statistical significance was determined by comparing the observed cluster statistics to a null distribution generated by randomly permuting the reported uncertainty across trials and repeating the analysis. For each permutation, the maximum cluster-level t-sum was recorded. This procedure was repeated 2,000 times to form the null distribution, and clusters exceeding the 95th percentile were considered significant. The same procedure was applied in Figure 4D to test the correlation between predicted uncertainty (from ridge regression on beta-band activity) and reported uncertainty.